Chemical Science

ROYAL SOCIETY OF CHEMISTRY

EDGE ARTICLE

View Article Online
View Journal | View Issue

Cite this: *Chem. Sci.*, 2025, **16**, 14262

All publication charges for this article have been paid for by the Royal Society of Chemistry

Dimerization of pillar[5]arene: length-adaptive encapsulation of long-chain guests†

Shunsuke Ohtani, *[a] Keigo Nakagawa,[a] Shigehisa Akine, [bc] Kenichi Kato [a] and Tomoki Ogoshi *[ac]

Encapsulation of long-chain molecules is challenging because host molecules must capture entire guest structures through interactions at multiple points. Cavitand and capsule molecules bind long-chain guests within their cavities, where long-chain guests adopt compressed conformations, to maximize interaction with the walls of the receptors. However, pillar[5]arene exhibits selective binding toward linear guest molecules in an extended chain conformation. It interacts more strongly with shorter guest molecules than with longer ones, as the shorter guests better match the length of the pillar-shaped cavity. Consequently, pillar[5]arene binds poorly to long-chain guest molecules that exceed its length. Herein, we synthesized pillar[5]arene dimers linked by phenyl and biphenyl linkers. Due to the cooperative binding provided by its two cavities, the biphenyl-linked dimer demonstrates length-adaptive behaviors for long-chain α,ω-dibromoalkanes that exceed its own length. This behavior is distinct from that of monomeric pillar[5]arene, which exhibits strict length-selectivity. Computational analysis suggests that the formation of curved host–guest complex structures with longer guests is facilitated by conformational adjustment of the biphenyl linker. Thermodynamic analyses reveal that enthalpic gains from the cooperative binding overcome entropic losses during the formation of the curved host–guest complexes, thus enabling length-adaptive binding for longer-chain guests.

Received 21st February 2025
Accepted 2nd July 2025

DOI: 10.1039/d5sc01403d

rsc.li/chemical-science

Introduction

Encapsulation of long-chain molecules is challenging because it requires capture of an entire structure through interactions at multiple points. Rebek's and Gibb's groups have shown that cavitand and capsule molecules can capture long-chain guests within their cavities (Fig. 1a).[1,2] In these cases, as the chain length increases, the longer-chain guests tend to adopt compressed arrangements, such as helical, J-shaped, and U-shaped conformations, to maximize their interactions with the walls of the receptors.[3–22]

Pillar[5]arene, a macrocyclic host first reported by our group in 2008, can accommodate aliphatic-chain guests in their extended conformation owing to its well-defined small cavity (Fig. 1b).[23–30] However, the length of the guest to be encapsulated is strictly determined by that of the pillar[5]arene structure, leading to a significant decrease in binding ability for alkane guests with five or more carbon units (Fig. 1c, S18–S20 and Table S1†). This is because the most electron-deficient methylene groups of the guests, located near the electron-withdrawing end groups, interact with the oxygen atoms on the rims of pillar[5]arene (Fig. S21†).[29,30] However, this strict length-selectivity prevents the capture of guests with lengths exceeding that of the pillar[5]arene in their extended conformation.

Constructing longer tubular structures based on pillar[5]arene enables the encapsulation of longer guest molecules because the host's multiple cavities can present cooperative binding sites for one guest.[31–36] For instance, our group prepared a pillar[5]arene cavitand end-capped with five linkers.[34] Sue and coworkers constructed rigid nanotubular hosts by connecting two pillar[5]arenes[35,36] that exhibit length-dependent host–guest interactions with α,ω-dibromoalkanes. Such well-defined tubular structures enable efficient binding for long-chain guests by minimizing the entropy loss due to rigidity, resulting in high association constants with suitable-length guests. However, there is still a limitation where the length of the tubular structure determines the length of guest, leading to reduced binding ability for long-chain guests that exceed the length of the host structure.

In this study, we constructed tubular structures by connecting two pillar[5]arenes with single linkers that make them

[a]*Department of Synthetic Chemistry and Biological Chemistry, Graduate School of Engineering, Kyoto University, Katsura, Nishikyo-ku, Kyoto, 615-8510, Japan. E-mail: otani.shunsuke.6k@kyoto-u.ac.jp; ogoshi.tomoki.3s@kyoto-u.ac.jp*

[b]*Graduate School of Natural Science and Technology, Kanazawa University, Kakuma-machi, Kanazawa, 920-1192, Japan*

[c]*WPI Nano Life Science Institute (WPI-NanoLSI), Kanazawa University, Kakuma-machi, Kanazawa, 920-1192, Japan*

† Electronic supplementary information (ESI) available. CCDC 2409580 and 2409578. For ESI and crystallographic data in CIF or other electronic format see DOI: https://doi.org/10.1039/d5sc01403d

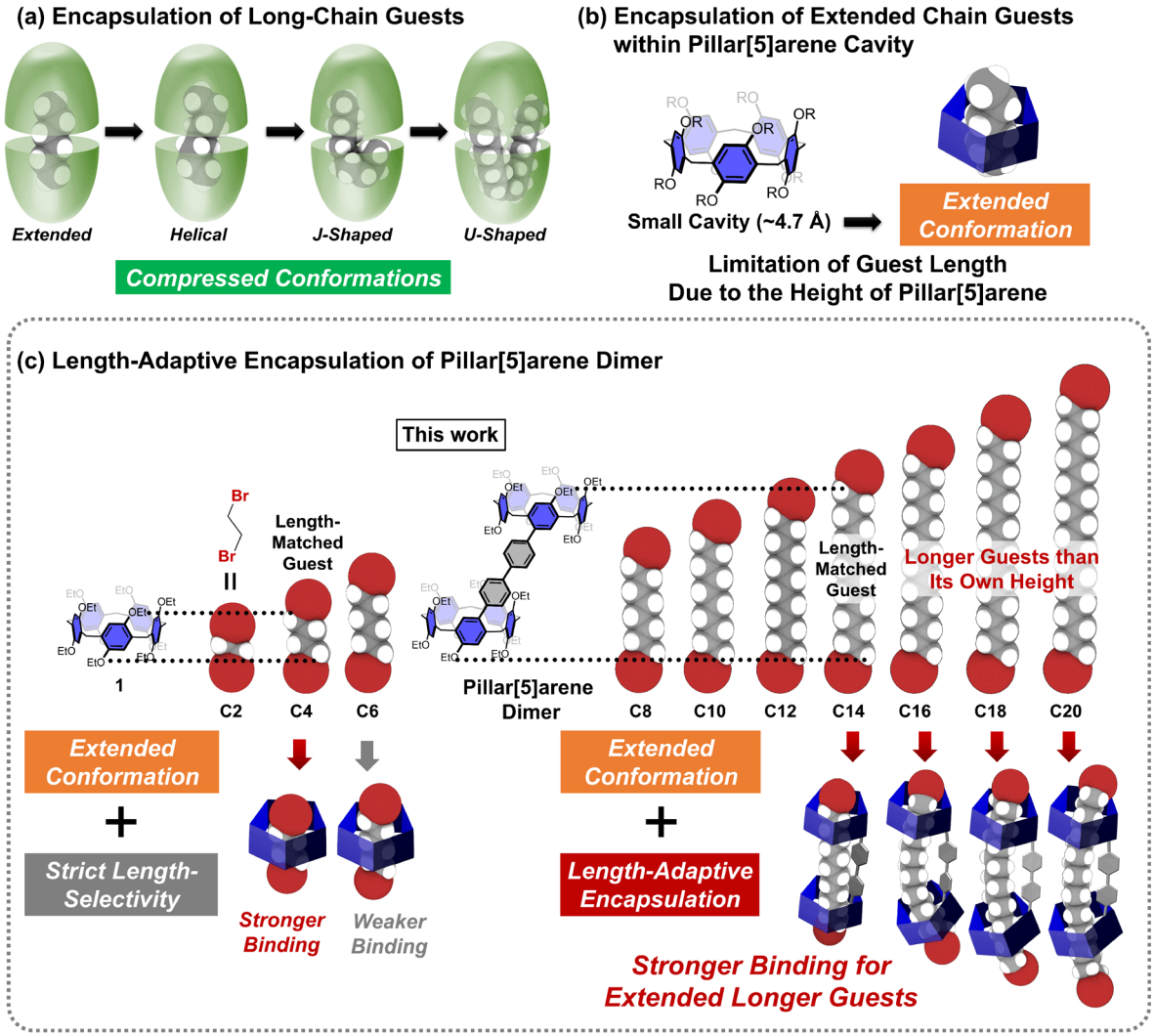

Fig. 1 Schematic representations of (a) encapsulation of long-chain guests by capsule molecules, (b) encapsulation of extended chain guests within pillar[5]arene cavity and (c) dimerization approach to extend the guest length beyond the limitation in this work.

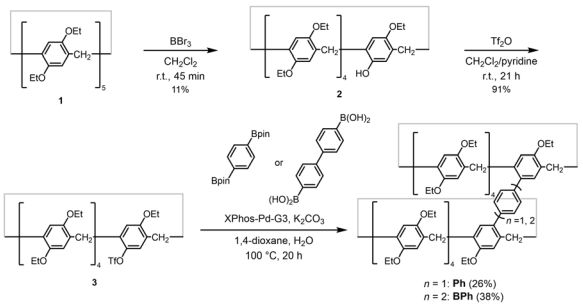

Scheme 1 Synthetic scheme for the pillar[*n*]arene dimers **Ph** and **BPh**.

adaptive (Fig. 1c). The key to achieving this is a delicate balance of rigidity and flexibility. Therefore, we selected phenylene linkers, as they were anticipated to minimize entropy loss during host–guest complexation, while still allowing rotation and moderate curving of the π-conjugated backbone. Although the two cavities of a monophenyl linked dimer do not exhibit cooperative binding due to steric hindrance, the biphenyl-linked version achieves cooperative binding for long-chain α,ω-dibromoalkanes. Notably, this system demonstrates length-adaptive binding for guests with 16 or more carbon units through conformational adjustment of the biphenyl linker, overcoming its intrinsic length limitation (Fig. 1c).

Results and discussion

Synthesis and single-crystal X-ray diffraction analysis

Perethoxylated pillar[5]arene **1** was employed as a starting compound for the synthesis of phenyl- and biphenyl-linked pillar[5]arene dimers **Ph** and **BPh**, as it shows better solubility in organic solvents compared to the permethoxylated analogue. In the final step, **Ph** and **BPh** were synthesized in 26% and 38% yields, respectively, by Suzuki–Miyaura cross-coupling of mono-triflated pillar[5]arene **3** [37] with 1,4-benzenediboronic acid bis(pinacol) ester or 4,4′-biphenyldiboronic acid (Schemes 1

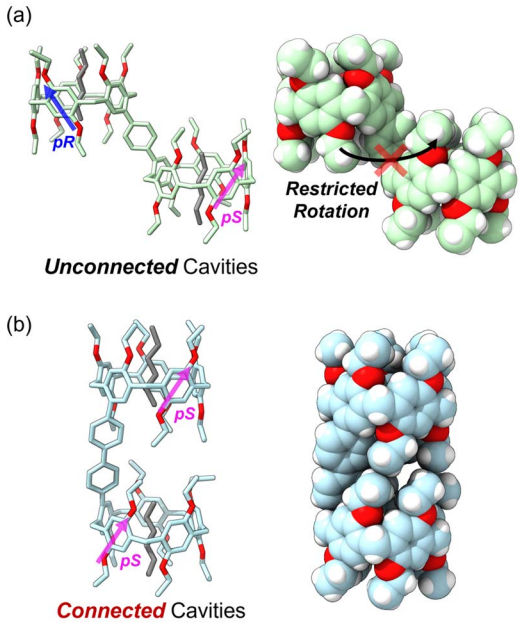

Fig. 2 Single-crystal X-ray structures (left: stick model; right: space-filling model) of (a) **Ph** and (b) **BPh** (*green* or *blue* carbon atoms; *red* oxygen atoms; *white* hydrogen atoms). Hexane molecules within the cavities are shown in gray.

and S1–S3†). They were fully characterized by ^{1}H and ^{13}C NMR spectroscopies and high-resolution ESI-MS spectrometry (Fig. S1–S7†). Furthermore, the proton peaks were unambiguously assigned through ^{1}H–^{1}H COSY, HMQC, and HSQC two-dimensional NMR spectroscopy analyses (Fig. S8–S13†).

Single-crystal X-ray diffraction analysis revealed that **Ph** adopts a conformation involving two cavities located on opposite sides to the linker (Fig. 2a and Table S2†).[38] In this conformation, the two cavities are unconnected and exist independently of each other (*unconnected* conformation). Since the ethoxy groups orient parallel to the pillar-shaped cavities, their steric interaction inhibits close contact of the two cavities, which biases the *unconnected* conformation in the crystal structure (Fig. 2a, right).

As shown in Fig. 2b, **BPh** adopts a conformation whereby two cavities located on the same side of the linkage form two connected cavities (*connected* conformation). In contrast to that for **Ph**, when the two cavities are connected in the same direction, the biphenyl linker provides sufficient length to avoid steric hindrance from the ethoxy groups (Fig. 2b, right). Consequently, **BPh** can adopt the *connected* conformation to form one pseudo-cavity in the crystal structure (see ESI Note 1† for solution-state conformational study).[39] In both crystals, hexane molecules are encapsulated within the cavities, and they adopt an extended conformation owing to the small cavity of pillar[5]arene (Fig. 2, left).

Pillar[5]arene has planar chirality depending on the orientation of the alkoxy groups.[40] For the two pillar[5]arene cavities of **Ph**, their planar chirality is defined as (all-*pS*, all-*pR*), that is, **Ph** acts as a heterochiral dimer in the crystals (Fig. 2a) in the crystals. In contrast, the planar chirality of the two cavities of

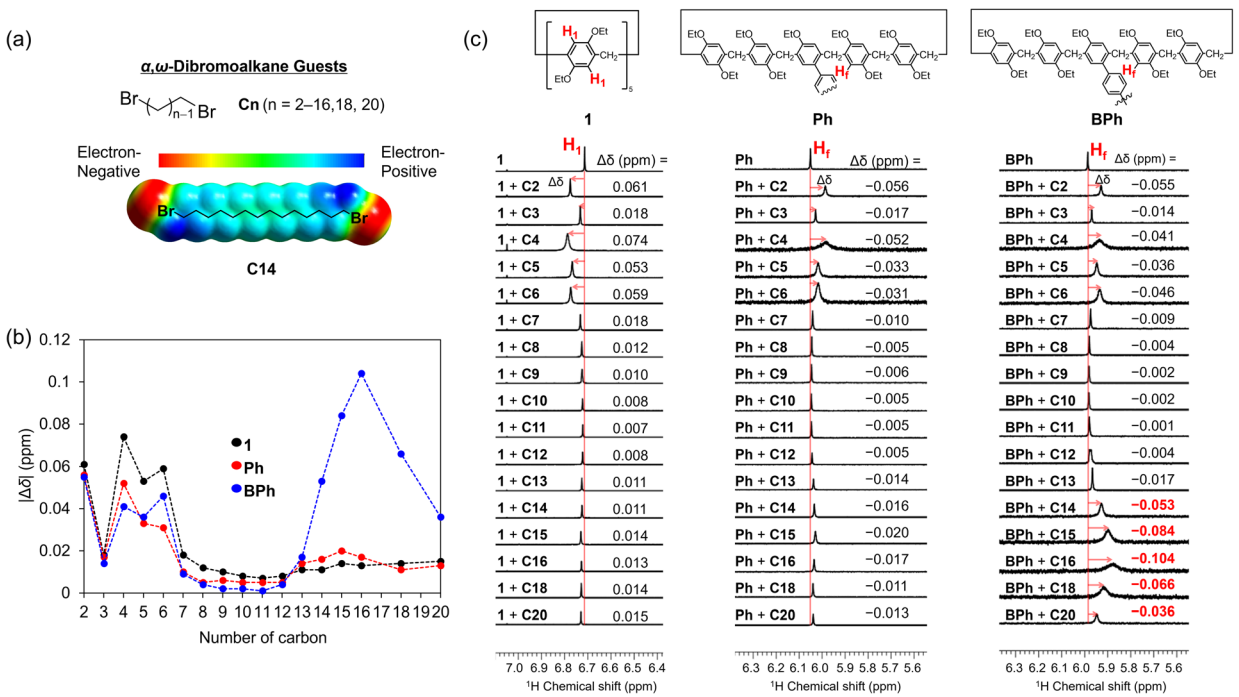

Fig. 3 (a) Chemical structures of α,ω-dibromoalkane guests and the electrostatic potential map of **C14** representing electron-deficient methylene moieties around the electron-withdrawing bromine atoms. (b) Plots of chemical-shift changes (Δδs) for the aromatic protons of **1**, **Ph**, and **BPh** (0.50 mM) with 1.0 eq. of α,ω-dibromoalkanes (**C2**–**C16**, **C18**, and **C20**) and (c) the corresponding ^{1}H NMR spectra (500 MHz, $CDCl_3$, 295 K) of **1**, **Ph**, and **BPh** with **C2**–**C16**, **C18** and **C20**.

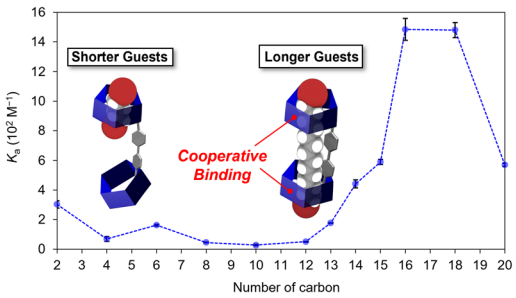

Fig. 4 Plot of the association constants (K_as) for **BPh** (1.0 mM, $CDCl_3$, 295 K) with α,ω-dibromoalkanes (**C*n***, n = 2, 4, 6, 8, 10, 12–16, 18, and 20). The illustrations depict 1 : 1 host–guest complexes of **BPh** with **C2** and **C14**, as suggested by Job's plots.

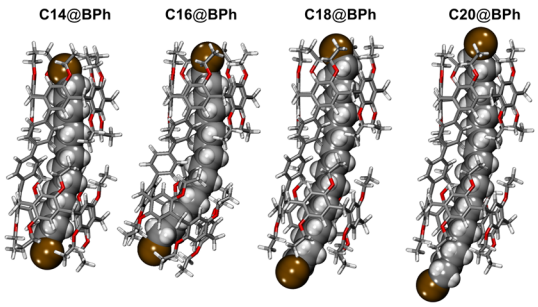

Fig. 5 Optimized geometries of host–guest complexes **C14@BPh**, **C16@BPh**, **C18@BPh**, and **C20@BPh** calculated at the M06-2X/6-31G(d,p) level of theory.

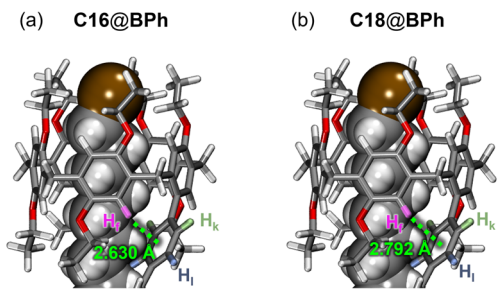

Fig. 6 Optimized geometries of (a) **C16@BPh** and (b) **C18@BPh** representing H_f, H_k and H_l atoms and the distances between H_f and aromatic ring of the linker.

BPh are (all-*pS*, all-*pS*) or (all-*pR*, all-*pR*), that is, **BPh** molecules act as homochiral dimers (Fig. 2b; see ESI Note 2† for details). This alignment of planar chirality facilitates close contacts between the ethoxy groups when **BPh** molecules adopt the *connected* conformation.

Host–guest behaviors of 1, Ph and BPh with α,ω-dibromoalkanes

To investigate the effect of *connected* and *unconnected* cavity conformations on the complexation, α,ω-dibromoalkane guests with different aliphatic chain lengths were explored. In this system, the electron-deficient methylene moieties around the electron-withdrawing bromine atoms interact with the electron-rich oxygen atoms on the rims of pillar[5]arene (Fig. 3a, S18 and S21 and Table S1†).

Initially, we measured the chemical-shift changes ($\Delta\delta$s) in ^{1}H NMR spectra when 1.0 eq. of α,ω-dibromoalkanes (**C*n***, n = 2–16, 18, and 20, Fig. 3a, S14–S17 and Schemes S4–S7†) were added to $CDCl_3$ solutions of monomeric pillar[5]arene (**1**), **Ph**, and **BPh** (Fig. 3b). The $\Delta\delta$s at aromatic protons of pillar[5]arene moieties were checked because the proton peaks of the guests became significantly broadened and disappeared after complexation. For **Ph** and **BPh**, the H_f peaks were selected because they showed the largest $\Delta\delta$s among all the host protons (Fig. S28†). This is due to the shielding of H_f protons from aromatic ring current in the linker moieties, resulting in upfield shifting compared to that for **Ph** and **BPh** without a guest (Fig. S26 and S27†). In all cases, comparable $\Delta\delta$ values were observed for shorter guests (**C2–C6**). Conversely, large $\Delta\delta$s were observed only for **BPh** complexes with longer guests (**C14–C16**, **C18**, and **C20**; blue dots in Fig. 3b). This clear trend suggests that the two cavities of **BPh** cooperatively capture one long guest in the *connected* conformation. **Ph** also has two cavities; however, they cannot work cooperatively because the *connected* conformation is unfavorable due to steric hindrance. As a result, similar $\Delta\delta$ values are observed with **1** (see ESI Note 3† for a detailed comparison of **1**, **Ph**, and **BPh** using their association constants (K_as) and Job's plots with short **C2** and long **C14** guests).

Host–guest behaviors of BPh with α,ω-dibromoalkanes

As observed with the $\Delta\delta$s for **1**, **Ph**, and **BPh**, only **BPh** shows a different chain-length dependence from those of **1** and **Ph**. In order to investigate that accurately, we determined K_as for α,ω-dibromoalkane guests with other chain lengths (Fig. 4 and S40–49†). For the shorter guests (**C2–C12**), the K_a values are low, which is consistent with the abovementioned results for $\Delta\delta$s (Fig. 3b). For longer guests, an increase is observed from **C13**. In particular, the K_a values for **C16** and **C18** reach $1.48 \pm 0.07 \times 10^3$ M^{-1} and $1.48 \pm 0.05 \times 10^3$ M^{-1}, respectively, which are four times higher than that for the **C2** guest. These observations demonstrate that cooperative binding enhances the binding abilities of pillar[5]arene, even for the longer guests.[41]

Length-adaptive behavior of BPh for longer guests

Considering the length of **BPh**, **C14** was expected to be a length-matched guest for **BPh** because the most electron-deficient moieties of **C14** would efficiently interact with the oxygen atoms of pillar[5]arene, as observed in the host–guest complexation of **1** with short guests (Fig. 1c and S18†). However, **BPh** shows increased K_a values for much longer guests (≥**C16**, Fig. 4).

To better understand the host–guest behavior of **BPh** for longer guests, we attempted single-crystal X-ray diffraction analyses of the host–guest complexes with longer guests. Regrettably, we could not obtain single crystals of these structures. Therefore, density functional theory (DFT) calculations were performed to estimate the structures of the host–guest

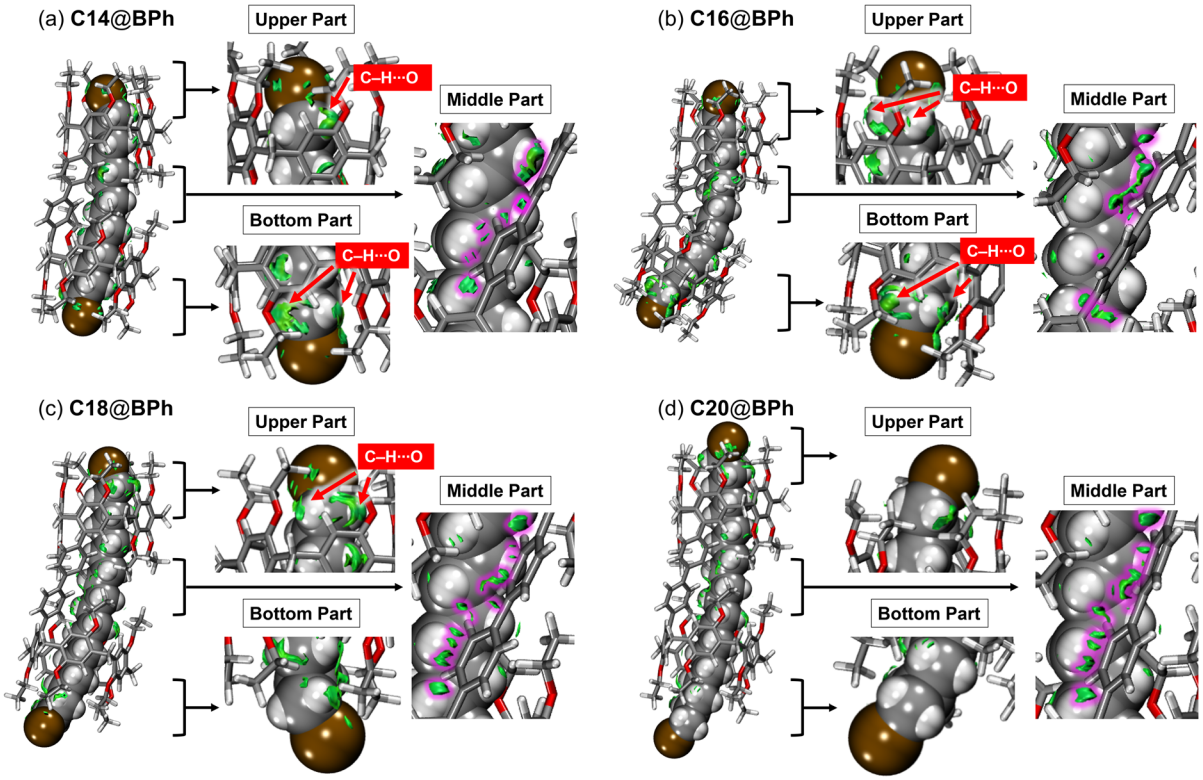

Fig. 7 Isosurfaces for (a) **C14@BPh**, (b) **C16@BPh**, (c) **C18@BPh**, and (d) **C20@BPh** calculated by IGMH analysis representing the non-covalent bonds in the upper, middle, and bottom parts (isovalues set equal to 0.007 a.u.). The isosurfaces between the biphenyl linker moieties and the middle parts of the guests are highlighted in pink.

Table 1 Thermodynamic parameters for the host–guest complexation of **1** with **C2**, **C3** and **C4**, and **BPh** with **C12**, **C14**, **C16**, **C18**, and **C20** (1.0 mM, $CDCl_3$)

Host	Guest	ΔG (kJ mol^{-1})	ΔH (kJ mol^{-1})	$T\Delta S^a$ (kJ mol^{-1})
1	**C2**	−18.7 ± 0.32	−51.7 ± 0.16	−33.0 ± 0.15
1	**C3**	−13.6 ± 8.6	−39.4 ± 4.4	−25.8 ± 4.2
1	**C4**	−22.3 ± 4.1	−68.1 ± 2.1	−45.8 ± 2.0
BPh	**C12**	—[b]	—[b]	—[b]
BPh	**C14**	−14.2 ± 9.0	−71.4 ± 4.5	−57.2 ± 4.4
BPh	**C16**	−17.2 ± 1.3	−88.8 ± 0.66	−71.6 ± 0.65
BPh	**C18**	−17.2 ± 2.5	−91.6 ± 1.3	−74.4 ± 1.3
BPh	**C20**	−15.0 ± 5.8	−78.5 ± 3.0	−63.5 ± 3.0

[a] $T = 298$ K. [b] Thermodynamic parameters could not be determined due to the low K_a value of **C12@BPh**.

complexes of **BPh** (**C14@BPh**, **C16@BPh**, **C18@BPh**, and **C20@BPh**).

In their optimized geometries (Fig. 5), curving of the guests and **BPh** occurs when the guest-length increases, demonstrating the length-adaptive conformational changes of **BPh** for guest molecules exceeding that of itself. In addition to rotation of the benzene moieties in the linkers, curving of the biphenyl-linked structures also occurs (Fig. S50†), while accommodating the curved alkane structures around the biphenyl linker. These host–guest complex structures are consistent with the experimentally estimated structures using ^{1}H NMR spectra recorded at 233 K (see ESI Note 4† for a detailed discussion for the host–guest complex structures).

The curved structure of **BPh** allows the H_f atom to come closer to the aromatic ring of the linkers (Fig. 6 and S66b†). Consequently, H_f is more shielded in the NMR spectra due to aromatic ring current, leading to upfield shifting compared to that for **BPh** without a guest (Fig. 3b). In response to that, H_k and H_l at the linker are deshielded, supporting the idea that H_f is shielded by the aromatic ring current of the linkers (Fig. S67†). The largest upfield-shift is observed for **C16** in the experimental ^{1}H NMR spectrum, despite the fact that the K_a is comparable with that for **C18** (Fig. 3b). This is because the more curved structure of **C16@BPh** allows the H_f atom to come closer to the aromatic ring (compared with that for **C18@BPh**; Fig. 6), which is supported by the DFT results calculated using the optimized geometries, *i.e.*, the calculated chemical shift for **C16@BPh** being upfield compared with that for **C18@BPh** (Fig. S66a and see ESI Note 5† for computational details). This result clearly demonstrates that the host–guest complexes of **BPh** with longer guests adopt the curved structures, as suggested by the computational results.

Non-covalent bonds in host–guest complexes of BPh

To visualize the non-covalent bonds between **BPh** and the guests, independent gradient-model based on Hirshfeld partition (IGMH) calculations were performed.[42,43] The green

isosurfaces indicate the presence of non-covalent bonds (Fig. 7). The visualized isosurfaces reveal the presence of C–H···O and C–H···Br interactions near the end groups of the guests, as well as van der Waals interaction around the linker. Among these interactions, a distinct difference is observed for the C–H···O interactions between **C14@BPh** and **C16@BPh**. For **C14@BPh**, isosurfaces are observed in three of the four most electron-deficient hydrogens at the α and ω positions for the bromine atoms (Fig. 7a). In contrast, those for **C16@BPh** are observed for all hydrogens at the α and ω positions (Fig. 7b), suggesting stronger non-covalent bonds than those for **C14@BPh**. This is because curving of both **BPh** and the guest allows closer contact between the cavities and the end parts of the guests. This optimization is also reflected in the closer distances between the hydrogen and oxygen atoms of **C16@BPh** compared with those for **C14@BPh** (Fig. S68†). In the case of **C18@BPh**, the isosurface is less distributed over one end part of the guest due to elongation of the aliphatic chain (the bottom end part of **C18** in Fig. 7c). Instead, non-covalent bonds between the biphenyl linker moieties and the guest become more distributed than those for **C14@BPh** and **C16@BPh** (Fig. 7). This can be explained by the fact that the curved guest aligns along the tilt of the biphenyl linker. For **C20@BPh**, an isosurface is scarcely observed over one end part of the guest (the bottom end part of **C20** in Fig. 7d) because one of the pillar[5]arene cavities cannot approach the end part of the guest, even though the **BPh** moiety is curved.

Comparison of thermodynamic parameters between BPh and 1 in the host–guest complexation

Finally, we compared the entropy and enthalpy changes (ΔS and ΔH, respectively) of **BPh** with those of monomeric pillar[5]arene **1** (Fig. S69–S82†).[44] As shown in Table 1, the host–guest complexations of both **BPh** and **1** are enthalpy-driven bindings. The enthalpic gains for **BPh** are greater than those for **1**. This is attributed to the two-cavity binding of **BPh**, where abundant non-covalent bonds contribute significantly to the enthalpic gains. Furthermore, optimization of the non-covalent bonds of **BPh** with **C16** and **C18** contribute to the enhancement of ΔHs, which is consistent with the above-mentioned computational results.[45]

Accordingly, greater entropy losses are observed for **BPh** compared with those for **1**. This can be explained by two reasons: (1) the degree of freedom for **BPh** in the uncomplexed state is higher than that for **1** because the linker of **BPh** can rotate in the solution.[46] (2) The abundant non-covalent bonds for the two-cavity binding in the complexed structures of **BPh** contribute to restriction of the molecular motions of **BPh** and guests, resulting in a more significant reduction in the degree of freedom than that for **1**.

In the enthalpy–entropy compensation plots (Fig. S83†), the linear relationship of $T\Delta S$ *versus* ΔH is defined as $T\Delta S = \beta\Delta H + T\Delta S_0$.[47–49] β shows the quantitative degree of conformational change upon host–guest complexation. The slope β of **BPh** is higher than that for **1** (**BPh**: $\beta = 0.83 \pm 0.02$; **1**: $\beta = 0.70 \pm 0.05$), which is greater than those of other conventional hosts (*e.g.*, flexible crown ether: $\beta = 0.76$; rigid cryptand: $\beta = 0.51$).[48] These results may indicate that **BPh** is more flexible and adaptive than **1** during host–guest complexation due to the adjustability of the biphenyl linker.

Conclusions

In summary, we synthesized pillar[5]arene dimers with aromatic linkers. By tuning of the linker length, the biphenyl-linked dimer shows host–guest behaviors for long α,ω-dibromoalkane guests with 14 carbon atoms owing to the cooperative binding across its two cavities. Notably, it still shows binding behaviors even for guests of lengths longer than its own, demonstrating length-adaptive binding. This behavior is totally different from that of monomeric pillar[5]arene, which shows strict length-selectivity for alkane guests. Computational and thermodynamic analyses revealed that the length-adaptive nature plays a crucial role in capturing longer guests with 16 or more carbon atoms.

Bindings of long-chain guests by previous synthetic receptors are often dependent on the volume of the hosts because the long guests are taken up in compressed conformations. These binding motifs are complex and difficult to control through molecular design. In contrast, our pillar[5]arene dimer can capture long-chain guests in the linearly extended conformations, offering a more predictable and tunable binding strategy. Importantly, our dimeric approach using pillar[5]arene has extensibility, allowing encapsulation of much longer aliphatic-chain guests by extending dimers to trimers, tetramers, and beyond. By employing our strategy, the range of guest lengths that can be captured is easily extended by varying the number of linked pillar[5]arenes. Increasing the number of linked pillar[5]arenes will enable the efficient complexation with linear polymers, unlocking new opportunities for the development of functional polymeric materials.

Data availability

Electronic supplementary information (ESI†) available: Synthetic procedures, NMR spectra, ESI-MS spectra, computational details, and X-ray structure details. CCDC 2409580 (**Ph**) and CCDC 2409578 (**BPh**).

Author contributions

Tomoki Ogoshi and Shunsuke Ohtani conceptualized and supervised the work. Keigo Nakagawa and Shigehisa Akine designed and performed experiments. The first draft of the manuscript was written by Keigo Nakagawa, Shunsuke Ohtani, and Tomoki Ogoshi. All authors analyzed and discussed the results, and co-wrote the paper.

Conflicts of interest

There are no conflicts to declare.

Acknowledgements

This work was supported by JST CREST Grant Number JPMJCR24S6 (T. O.), Japan, JSPS KAKENHI Grant Numbers JP22K14725 (Early-Career Scientists, S. O.), JP22K19063 (Challenging Research (Exploratory), T. O.), JP22H00334 (Scientific Research (A), T. O.), JP24K21247 (Challenging Research (Pioneering), T. O.), and the MEXT World Premier International Research Center Initiative (WPI), Japan. Computation time was provided by the SuperComputer System, Institute for Chemical Research, Kyoto University. We thank Dr Jay Freeman at Edanz (**https://jp.edanz.com/ac**) for editing a draft of this manuscript.

Notes and references

1 A. Scarso, L. Trembleau and J. Rebek Jr, *Angew. Chem., Int. Ed.*, 2003, **42**, 5499–5502.
2 C. L. Gibb and B. C. Gibb, *Chem. Commun.*, 2007, 1635–1637.
3 L. Trembleau and J. Rebek Jr, *Science*, 2003, **301**, 1219–1220.
4 A. Scarso, L. Trembleau and J. Rebek Jr, *J. Am. Chem. Soc.*, 2004, **126**, 13512–13518.
5 Y. H. Ko, H. Kim, Y. Kim and K. Kim, *Angew. Chem., Int. Ed.*, 2008, **47**, 4106–4109.
6 S. Liu, D. H. Russell, N. F. Zinnel and B. C. Gibb, *J. Am. Chem. Soc.*, 2013, **135**, 4314–4324.
7 K.-D. Zhang, D. Ajami, J. V. Gavette and J. Rebek Jr, *J. Am. Chem. Soc.*, 2014, **136**, 5264–5266.
8 S. Mosca, D. Ajami and J. Rebek Jr, *Proc. Natl. Acad. Sci. U. S. A.*, 2015, **112**, 11181–11186.
9 J. W. Barnett, B. C. Gibb and H. S. Ashbaugh, *J. Phys. Chem. B*, 2016, **120**, 10394–10402.
10 R. Z. Pavlovic, S. E. Border, T. J. Finnegan, L. Zhiquan, M. J. Gunther, E. Mu Noz, C. E. Moore, C. M. Hadad and J. D. Badjic, *J. Am. Chem. Soc.*, 2019, **141**, 16600–16604.
11 K. Harada, R. Sekiya and T. Haino, *J. Org. Chem.*, 2021, **86**, 4440–4447.
12 J. Scelle, H. Vervoitte, L. Bouteiller, L. M. Chamoreau, M. Sollogoub, G. Vives and B. Hasenknopf, *Chem. Sci.*, 2022, **13**, 2218–2225.
13 D. Dumitrescu, Y. M. Legrand, E. Petit, A. van der Lee and M. Barboiu, *Chem. Sci.*, 2015, **6**, 2079–2086.
14 D. Ajami and J. Rebek Jr, *Acc. Chem. Res.*, 2013, **46**, 990–999.
15 D. Ajami and J. Rebek Jr, *Nat. Chem.*, 2009, **1**, 87–90.
16 K. Niki, T. Tsutsui, M. Yamashina, M. Akita and M. Yoshizawa, *Angew. Chem., Int. Ed.*, 2020, **59**, 10489–10492.
17 R. E. Fadler, A. Al Ouahabi, B. Qiao, V. Carta, N. F. Konig, X. Gao, W. Zhao, Y. Zhang, J. F. Lutz and A. H. Flood, *J. Org. Chem.*, 2021, **86**, 4532–4546.
18 Q. Sun, L. Escobar and P. Ballester, *Angew. Chem., Int. Ed.*, 2021, **60**, 10359–10365.
19 J. M. Yang, Y. Q. Chen, Y. Yu, P. Ballester and J. Rebek Jr, *J. Am. Chem. Soc.*, 2021, **143**, 19517–19524.
20 W. Zhao, B. Qiao, J. Tropp, M. Pink, J. D. Azoulay and A. H. Flood, *J. Am. Chem. Soc.*, 2019, **141**, 4980–4989.
21 L. Escobar and P. Ballester, *Chem. Rev.*, 2021, **121**, 2445–2514.
22 Y. Akae, H. Sogawa and T. Takata, *Eur. J. Org Chem.*, 2019, **2019**, 3605–3613.
23 T. Ogoshi, S. Kanai, S. Fujinami, T. Yamagishi and Y. Nakamoto, *J. Am. Chem. Soc.*, 2008, **130**, 5022–5023.
24 T. Ogoshi, T. Yamagishi and Y. Nakamoto, *Chem. Rev.*, 2016, **116**, 7937–8002.
25 X. B. Hu, L. Chen, W. Si, Y. Yu and J. L. Hou, *Chem. Commun.*, 2011, **47**, 4694–4696.
26 Z. Zhang, B. Xia, C. Han, Y. Yu and F. Huang, *Org. Lett.*, 2010, **12**, 3285–3287.
27 T. Ogoshi, R. Sueto, K. Yoshikoshi, Y. Sakata, S. Akine and T. Yamagishi, *Angew. Chem., Int. Ed.*, 2015, **54**, 9849–9852.
28 X. Shu, S. Chen, J. Li, Z. Chen, L. Weng, X. Jia and C. Li, *Chem. Commun.*, 2012, **48**, 2967–2969.
29 X. Shu, J. Fan, J. Li, X. Wang, W. Chen, X. Jia and C. Li, *Org. Biomol. Chem.*, 2012, **10**, 3393–3397.
30 C. Li, S. Chen, J. Li, K. Han, M. Xu, B. Hu, Y. Yu and X. Jia, *Chem. Commun.*, 2011, **47**, 11294–11296.
31 T. Ogoshi, K. Demachi, K. Kitajima and T. Yamagishi, *Chem. Commun.*, 2011, **47**, 10290–10292.
32 N. L. Strutt, H. Zhang, S. T. Schneebeli and J. F. Stoddart, *Chem.–Eur. J.*, 2014, **20**, 10996–11004.
33 C. Li, K. Han, J. Li, H. Zhang, J. Ma, X. Shu, Z. Chen, L. Weng and X. Jia, *Org. Lett.*, 2012, **14**, 42–45.
34 T.-H. Shi, Y. Nagata, S. Akine, S. Ohtani, K. Kato and T. Ogoshi, *J. Am. Chem. Soc.*, 2022, **144**, 23677–23684.
35 Y. Tian, Y. Guo, X. Dong, X. Wan, K.-H. Cheng, R. Chang, S. Li, X. Cao, Y.-T. Chan and A. C.-H. Sue, *Nat. Synth.*, 2023, **2**, 395–402.
36 S. Gao, Y. Guo, J. Xue, X. Dong, X. Y. Cao and A. C.-H. Sue, *J. Am. Chem. Soc.*, 2024, **146**, 20963–20971.
37 T. Kaneda, K. Kato, S. Ohtani and T. Ogoshi, *Bull. Chem. Soc. Jpn.*, 2024, **97**, uoae093.
38 Deposition numbers 2409580 (for **Ph**) and 2409578 (for **BPh**) contain the supplementary crystallographic data for this paper.
39 With the phenyl linker, the two cavities are close to each other, making it difficult to adopt the *connected* conformation even if the ethoxy groups were replaced with methoxy groups.
40 T. Ogoshi, R. Shiga, T. Yamagishi and Y. Nakamoto, *J. Org. Chem.*, 2011, **76**, 618–622.
41 With a flexible alkyl linker, achieving efficient cooperative binding would likely be challenging due to the entropic disadvantage. Furthermore, since cooperative binding is already achieved with the biphenyl linker, employing longer phenylene linkers would likely facilitate the encapsulation of much longer guests.
42 T. Lu and F. Chen, *J. Comput. Chem.*, 2012, **33**, 580–592.
43 T. Lu and Q. Chen, *J. Comput. Chem.*, 2022, **43**, 539–555.
44 The K_a of **1** decreases for longer guests, whereas that of **BPh** decreases for shorter guests. Since sufficiently large K_as are required to calculate the thermodynamic parameters, comparisons between **1** and **BPh** cannot be made using the same guests.
45 In addition to the strength of non-covalent bonds, ΔH values are also contributed from the strain energy changes of **BPh**

and guests during host–guest complexations. However, computational analyses suggest that the total strain energy changes are not significantly different between **C14@BPh**, **C16@BPh**, **C18@BPh**, and **C20@BPh** (Table S4†). Consequently, differences in ΔH values are mainly arisen from the varying degrees of non-covalent bonds between **BPh** and guests.

46 As the chain length of the guests becomes longer, the degrees of freedom increase. Consequently, in the case of **BPh**, the encapsulation of the longer guests significantly reduces their freedom, resulting in greater entropy loss compared to **1**.

47 Y. Inoue and T. Hakushi, *J. Chem. Soc., Perkin Trans. 2*, 1985, 935–946.

48 Y. Inoue, Y. Liu, L. H. Tong, B. J. Shen and D. S. Jin, *J. Am. Chem. Soc.*, 1993, **115**, 10637–10644.

49 D. Shimoyama and T. Haino, *Chem.–Eur. J.*, 2020, **26**, 3074–3079.